2-13-2012

Biophysical characterization of a riboflavin-conjugated dendrimer platform for targeted drug delivery

Amanda B. Witte
Calvin University

Christine M. Timmer
Calvin University

Jeremy J. Gam
Michigan Medicine

Seok Ki Choi
Michigan Medicine

Article

pubs.acs.org/Biomac

Biophysical Characterization of a Riboflavin-Conjugated Dendrimer Platform for Targeted Drug Delivery

Amanda B. Witte,[†] Christine M. Timmer,[†] Jeremy J. Gam,[‡] Seok Ki Choi,*[,‡] Mark M. Banaszak Holl,[‡,§,⊥,#] Bradford G. Orr,[‡,∥] James R. Baker, Jr.,*[,‡,⊥] and Kumar Sinniah*[,†]

[†]Department of Chemistry & Biochemistry, Calvin College, 3201 Burton Street South East, Grand Rapids, Michigan 49546, United States

[‡]Department of Internal Medicine, Michigan Nanotechnology Institute for Medicine and Biological Sciences, [§]Department of Chemistry, [∥]Department of Physics, [⊥]Department of Biomedical Engineering, and [#]Department of Macromolecular Science and Engineering, University of Michigan, Ann Arbor, Michigan 48109, United States

Supporting Information

ABSTRACT: The present study describes the biophysical characterization of generation-five poly(amidoamine) (PAMAM) dendrimers conjugated with riboflavin (RF) as a cancer-targeting platform. Two new series of dendrimers were designed, each presenting the riboflavin ligand attached at a different site (isoalloxazine at N-3 and D-ribose at N-10) and at varying ligand valency. Isothermal titration calorimetry (ITC) and differential scanning calorimetry (DSC) were used to determine the binding activity for riboflavin binding protein (RfBP) in a cell-free solution. The ITC data shows dendrimer conjugates have K_D values of ≥465 nM on a riboflavin basis, an affinity ~93-fold lower than that of free riboflavin. The N-3 series showed greater binding affinity in comparison with the N-10 series. Notably, the affinity is inversely correlated with ligand valency. These findings are also corroborated by DSC, where greater protein−conjugate stability is achieved with the N-3 series and at lower ligand valency.

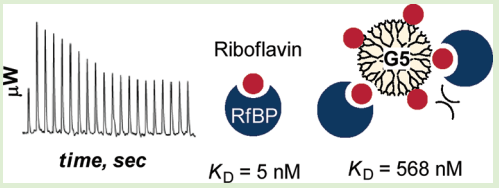

INTRODUCTION

Multivalency provides the biophysical basis for the mechanism of cell targeting in targeted drug delivery.[1−6] The targeting effectiveness of the delivery system is frequently predicted by determining its avidity constant in vitro, a collective property that measures the strength of multivalent association between multiple receptor−ligand pairs.[3] However, the affinity constant that measures the strength of the monovalent interaction for an independent receptor−ligand pair is far less studied despite its direct influence on the avidity. In this Article, we investigate the biophysical aspects of monovalent interactions with a cancer-targeting system comprising the riboflavin (RF)-presenting multivalent dendrimer[7] and the soluble RF receptor. We address the thermodynamic parameters, affinity, and stability as a function of design factors including ligand valency and orientation. The present study strongly suggests that evaluation of monovalent interactions also provides important information that should be taken into consideration in the design process of a multivalent delivery system.

Recent advances in nanotechnology have led to the discovery of various multifunctional platforms applicable for targeted drug delivery in many critical therapeutic areas from cancers to inflammatory diseases.[8−13] These delivery platforms are typically composed of a nanometer-sized carrier conjugated with multiple copies of a cell targeting ligand and also a payload of small molecule chemotherapeutics, therapeutic genes, and imaging agents. Multifunctional platforms enable selective uptake of the payload by pathological cells and therefore improve their therapeutic indices of treatments.[8−13] Applications of this approach for anticancer therapeutic molecules have been extensively investigated by the targeting of cancer-specific surface biomarkers such as folic acid receptor-α (FAR$_\alpha$),[14,15] RF receptor,[7,16] $\alpha_v\beta_3$ integrin,[2,17,18] prostate-specific membrane antigen,[19] Her2 receptor,[20] transferrin receptor,[21] and epidermal growth factor receptor.[20,22,23]

We have recently begun to explore RF as a small molecule ligand for the targeted delivery of anticancer therapeutic agents.[7,16] RF receptors are overexpressed in certain cell lines including human breast and prostate cancers, and this family of proteins potentially constitutes one type of tumor biomarker.[24,25] In our previous approach, we designed a novel delivery platform based on a fifth-generation (G5) poly(amidoamine) (PAMAM) dendrimer[26,27] conjugated with the RF ligand (Figure 1), which demonstrated the targeted delivery of the anticancer drug methotrexate (MTX) in KB cancer cells in vitro.[7] This preliminary work points to the possibility of other similar applications against cancer cells that overexpress the RF receptors.

Here we were interested in investigating the basic design principles of a RF-conjugated PAMAM dendrimer by using biophysical techniques to identify its optimal design features. We focused on two design factors, ligand orientation and valency, because they are known to make significant contributions to controlling the avidity of the multivalent

Received: November 6, 2011
Revised: December 16, 2011
Published: December 22, 2011

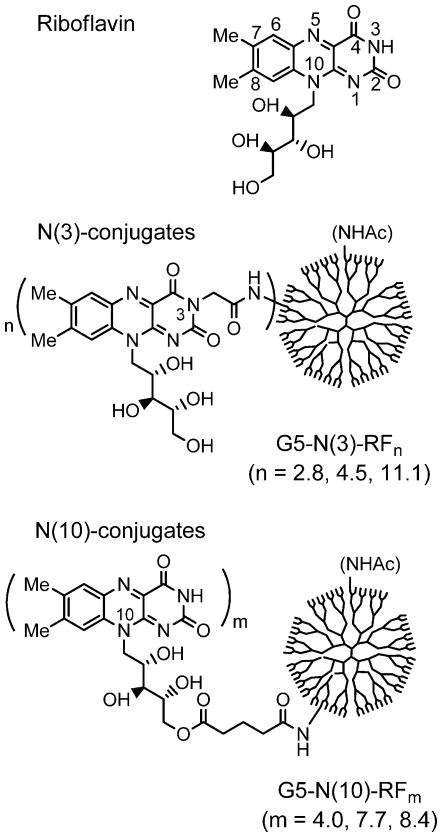

Figure 1. Structures of RF and two series of RF dendrimer conjugates used in present study. In each series, the RF ligand is tethered to the G5 PAMAM dendrimer through a linker located at its N-3 or N-10 position.

ligand.[3] First, we attached the RF ligand in two distinct orientations. This is because the structure of a RF molecule contains two orthogonal domains, each amenable for chemical modifications required for the dendrimer conjugation: an N-3 position at an isoalloxazine head and a (D)-ribose unit attached at the N-10 position (Figure 1). According to the only crystal structure determined for RF in complex with chicken riboflavin binding protein (RfBP),[28] the xylene domain of the isoalloxazine head is stacked between hydrophobic planes comprising the RF binding cleft, and the (D)-ribose unit is exposed to the aqueous medium. Therefore, either the N-3 position of the isoalloxazine head[16] or the primary alcohol at the (D)-ribose[7,29,30] can be utilized as a tethering site. This structure-guided design strategy suggests the comparison of the two ligand orientations in terms of the linker attachment: the N-3 position and the (D)-ribose linked to the N-10 position, which was already employed in our prior study[7] (Figure 1). The linker length for each RF attachment is relatively short. However, our prior studies based on cellular binding[7] and the surface plasmon resonance (SPR) study[16] demonstrated that the linker length was long enough for the dendrimer-attached RF to bind the targeted receptor protein. Second, in each of the linker series (N-3, N-10), we varied the average number of RF ligands tethered to the dendrimer to determine how such variation makes an impact on the dissociation constant (K_D) of the tethered RF ligand to mammalian RfBP acting as the model receptor.

The dissociation constant (K_D) we measured here refers to the affinity constant for the independent, monovalent ligand–receptor interactions. It is thus different from the avidity constant, a collective property that indicates the strength of the multivalent interaction as previously noted.[3] The avidity can be measured by several biophysical methods including SPR spectroscopy[1,16] and cell-based fluorescence assays.[7,30] Such methods have already demonstrated the positive correlation between the avidity and the ligand valency.[1,2,8,31−33] Despite the advantages for measuring such collective properties, each of these methods has limitations in providing direct information on the strength of discrete monovalent interactions. This Article employs two other complementary techniques, isothermal titration calorimetry (ITC) and differential scanning calorimetry (DSC), to address the thermodynamic aspects of the monovalent receptor–ligand interactions for two series of RF-conjugated dendrimers, each having a variable valency of the ligand attached at a different RF site (N-3, N-10). Here we report the identification of a preferred position for the RF attachment, and an optimal range of ligand valency. More notably, we find that the affinity for the RF ligand decreases significantly both upon its covalent attachment to the dendrimer and as a function of ligand valency.

EXPERIMENTAL SECTION

Materials. RF binding protein, apo-form was purchased from Sigma-Aldrich (CAS 91386-80-0). Phosphate-buffered saline (PBS) and 1.0 M phosphate buffer were purchased from Sigma-Aldrich. (−)-RF (purity ≥98%) and fluorescein 5(6)-isothiocyanate (FITC; purity ∼90%) were purchased from Sigma-Aldrich. G5 poly(amidoamine) (PAMAM) dendrimer was purchased as a 17.5% (w/w) methanol solution (Dendritech, Midland, MI). The PAMAM dendrimer was purified by dialysis prior to use as described elsewhere.[34]

General Synthetic Methods. All solvents and reagents were purchased from commercial suppliers and used without further purification. Characterization of compounds was typically carried out by nuclear magnetic resonance (NMR) spectroscopy, mass spectrometry, and UV/vis spectrometry. For the NMR measurement, each sample was dissolved in a deuterated solvent (CD_3OD, D_2O), and its ^1H NMR spectrum was acquired with a Varian NMR spectrometer at 500 MHz under a standard observation condition. The molecular weights for a fifth-generation PAMAM dendrimer and its RF conjugates were measured by matrix-assisted laser desorption ionization-time-of-flight (MALDI TOF) with a Waters TOfsPec-2E spectrometer, as described elsewhere.[35] The spectrometer was mass-calibrated with BSA in sinapinic acid, and data were acquired and processed using Mass Lynx 3.5 software. UV–vis absorption spectra were recorded on a Perkin-Elmer Lambda 20 spectrophotometer.

The purity of each dendrimer conjugate was determined by HPLC, which was carried out on a Waters Acquity Peptide Mapping System equipped with a Waters photodiode array detector (a UPLC system).[35] Each sample solution was run on a C4 BEH column (150 × 2.1 mm, 300 Å) connected to Waters Vanguard column. Elution of the conjugate was performed in a linear gradient beginning with 98:2 (v/v) water/acetonitrile (with trifluoroacetic acid at 0.14 wt % in each eluent) at a flow rate of 1 mL/min.

Synthesis of G5-N(3)-RF$_n$ Conjugates 4–7 (n = 2.8, 4.5, 11.1). 3-Carboxymethylriboflavin **1** was synthesized as described elsewhere.[16,36,37] It was first converted to its activated NHS ester form **2** as follows. To a stirred solution of 3-carboxymethylriboflavin (27 mg, 63 μmol) dissolved in DMF (total volume = 5.5 mL) was added *N*-hydroxysuccinimide (NHS; 8 mg, 69 μmol), 4-dimethylaminopyridine (DMAP; 8 mg, 69 μmol), and *N*-(3-dimethylaminopropyl)-*N*′-ethylcarbodiimide hydrochloride (EDC; 13 mg, 69 μmol) in a sequence. The reaction mixture was stirred at ambient temperature for 12 h. Four separate glass vials were prepared, each containing G5 PAMAM dendrimer (30 mg, 1.1 μmol) dissolved in MeOH (10 mL). The solution of the activated ester **2** in DMF was divided into four

aliquots (2, 2, 1, and 0.5 mL), and each aliquot was added to each of the dendrimer solutions. Each reaction mixture was stirred for 2 days at rt. For conjugation with fluorescein isothiocyanate (FITC), one of the reaction mixtures, the one that contained 2 mL of the activated ester, was further treated by adding FITC (2 mg, 5.7 μmol) dissolved in methanol (1 mL). This mixture was stirred additionally for 1 day at rt. After the stirring, each of the above mixtures was treated with acetic anhydride (24 μL, 250 μmol) and triethylamine (35 μL, 250 μmol), and the final mixture was stirred for 6 h. As an illustration for a typical purification method, each reaction mixture was concentrated in vacuo, and the residue was dissolved in 10 mL of PBS (pH 7.4). The solution was loaded into a membrane dialysis bag (MWCO 10 kDa) and dialyzed against PBS (2 × 2 L) and deionized water (3 × 2 L) over 3 days until its dendrimer purity was greater than 95%, as determined by the anal. HPLC method (Figure S3 of the Supporting Information). The aqueous solution was collected and freeze-dried to afford the G5-N(3)-RF$_n$ as pale-yellow solid: **3** (29 mg), **4** (28 mg), **5** (26 mg), and **6** (23 mg). The number (valency) of RF ligands attached to the surface of the dendrimer was estimated on a mean basis by the analysis of ^{1}H NMR, UV/vis, and MALDI mass spectral data following the general method, as described elsewhere (Table S1 of the Supporting Information).[7,35] MALDI TOF mass spectrometry (m/z, g mol^{-1}): **4** (m/z = 33 400); **5** (m/z = 35 300); **6** (m/z = 36 900); 7 (m/z = 38 200). UV/vis (PBS, pH 7.2): **4**–**6**: λ_{max} = 449 nm (ε = 12 100 M^{-1} cm^{-1} calculated on the basis of RF), 272 nm (ε = 10 300 M^{-1} cm^{-1} calculated on the basis of RF); 7: λ_{max} = 491 nm (ε = 100 000 M^{-1}cm^{-1} calculated on the basis of FITC). ^{1}H NMR (500 MHz, D_2O): **4**: δ 8.07–7.88 (br q), 4.55–4.48 (br s), 4.34–4.26 (br s), 3.70–3.67 (br s), 3.49–3.39 (s), 3.17–3.05 (s), 2.74–2.64 (s), 2.61–2.59 (br s), 2.54–2.51 (quint), 2.51–2.42 (s), 2.27–2.17 (s), 2.03–2.01 (br s), 2.00–1.98 (br s), 1.98–1.97 (br s),1.89–1.88 (br s), 1.84–1.79 (s), 1.66–1.65 (br s); **5**: δ 8.19–8.17 (br s), 8.07–7.82 (br q), 4.54–4.49 (br s), 4.34–4.28 (br s), 3.70–3.66 (br s), 3.66–3.64 (br s), 3.59–6.56 (br s), 3.46–3.35 (s), 3.16–3.04 (s), 2.74–3.62 (s), 2.62–3.59 (br s), 2.54–2.50 (s), 2.50–2.41 (s), 2.26–2.17 (s), 1.89–1.87 (br s), 1.83–1.78 (s), 1.67–1.64 (br s); **6**: δ 8.2–8.13 (br s), 8.06–7.77 (t), 5.07–2.94 (br s), 4.76–2.62 (br s), 4.58–4.44 (br s), 4.35–4.21 (br s), 3.71–3.61 (br d), 3.47–3.34 (s), 3.21–3.02 (s), 2.77–2.62 (s), 2.62–2.57 (s), 2.56–2.50 (s), 2.50–2.36 (s), 2.29–2.05 (s), 1.87–1.74 (s); 7: δ 8.11–7.8 (br q), 6.71–6.55 (br d), 5.08–4.98 (br s), 4.74–4.64 (br s), 4.54–4.46 (br s), 4.35–4.25 (br s), 4.18–4.13 (br s), 3.71–3.66 (br s), 3.66–3.62 (br s), 3.60–3.54 (br s), 3.45–3.35 (s), 3.16–3.04 (s), 2.73–2.60 (s), 2.60–2.58 (br s), 2.54–2.48 (s), 2.48–2.38 (br s), 2.25–2.13 (s), 1.89–1.87 (br s), 1.83–1.77 (s), 1.33–1.27 (br s), 1.27–1.24 (br s), 0.90–0.85 (br d). HPLC: **4** (t_r = 7.70 min; purity = 95%); **5** (t_r = 7.79 min; purity = 97%); **6** (t_r = 7.91 min; purity = 98%); 7 (t_r = 8.30 min; purity = 97%).

Synthesis of G5-N(10)-RF$_m$ Conjugates 10–12 (m = 4.0, 7.7, 8.4). A suspension of RF (500 mg, 1.3 mmol) in a mixture of DMSO (5 mL) and pyridine (10 mL) was stirred at 90 °C until it became completely dissolved. To this hot solution was added glutaric anhydride (303 mg, 2.6 mmol) as solid. The mixture was stirred at the same temperature for 12 h, and it was concentrated in vacuo, yielding pale brown solid. This residue was thoroughly rinsed with ether and acetonitrile in multiple times and dried in vacuo to afford **8** as brown foam (472 mg, 73%). This crude product was used for the conjugation with the PAMAM dendrimer without further treatment. HRMS (ESI, negative ion mode): calcd for $C_{22}H_{26}N_4O_9$ [M-H]$^-$, m/z = 489.1627 (**8**), found 489.1620; calcd for $C_{27}H_{32}N_4O_{12}$[M-H]$^-$, m/z = 603.1938 (a diadduct of glutaric anhydride), found 603.1920.

To a solution of **8** (33 mg, 67 μmol) in DMF (4 mL) was added NHS (12 mg, 101 μmol), DMAP (16 mg, 135 μmol), and EDD (26 mg, 135 μmol) in a sequence. The reaction mixture was stirred at ambient temperature for 16 h. Three separate glass vials (20 mL capacity) were prepared, each containing G5 PAMAM dendrimer (25 mg, 1.0 μmol) dissolved in MeOH (10 mL). The DMF solution containing the activated ester **9** was divided to three aliquots (0.9, 1.3, and 1.8 mL), and each aliquot was added to each of the dendrimer solutions. Each reaction mixture was stirred for 2 d at rt and then treated with acetic anhydride (20 μL, 208 μmol) and triethylamine (29 μL, 208 μmol), and the final mixture was stirred for 6 h. As an illustrative method for purification, each reaction mixture was concentrated in vacuo, and the residue was dissolved in 10 mL of PBS (pH 7.4). The solution was loaded into a membrane dialysis bag (MWCO 10 kDa) and dialyzed against PBS (2 × 2 L), and deionized water (3 × 2 L) over 3 days until its dendrimer purity was greater than 95%, as determined by the anal. HPLC method (Figure S3 of the Supporting Information). The aqueous solution was collected and freeze-dried in vacuo to afford the G5-N(10)-RF$_m$ as pale-yellow solid: **10** (25 mg), **11** (28 mg), and **12** (30 mg). The number (valency) of RF ligands attached to the surface of the dendrimer was estimated on a mean basis by the analysis of ^{1}H NMR, UV/vis, and MALDI mass spectral data (Table S1 of the Supporting Information). MALDI TOF mass spectrometry (m/z, g mol^{-1}): **10** (m/z = 33 700); **11** (m/z = 36 900); **12** (m/z = 40 300). UV/vis (PBS, pH 7.2): **10**–**12**: λ_{max} = 449 nm (ε = 12 100 M^{-1} cm^{-1} calculated on the basis of RF), 374 nm (ε = 10 300 M^{-1}cm^{-1} calculated on the basis of RF). ^{1}H NMR (500 MHz, D_2O): **10**: δ 7.91–7.57(br s), 4.89–4.88 (br s), 4.85–4.84 (br s), 4.84–4.77 (s), 4.73–4.72 (br s), 4.46–4.39 (br s), 4.32–4.27 (br s), 4.21–4.15 (br s), 4.15–4.08 (br s), 4.02–3.96 (br s), 3.89–3.83 (br s), 3.72–3.67 (br s), 3.52–3.46 (br s), 3.45–3.13 (quint), 2.89–2.76 (s), 2.68–2.58 (s), 2.58–2.53 (br), 2.50–2.32 (s), 2.31–2.27 (br s), 2.25–2.22 (br), 2.19–2.16 (br), 2.14–2.13 (br s), 2.11–2.09 (br s), 2.05–2.04 (br s), 2.01–1.95 (s), 1.94–1.86 (br s), 1.86–1.80 (br), 1.27–1.25 (br s); **11**: δ 7.89–7.53 (br s), 5.61–5.49 (br s), 5.42–5.34 (br s), 5.29–5.23 (br s), 4.89–4.87 (s), 4.85–4.76 (br), 4.45–4.37 (br), 4.34–4.27 (br s), 4.22–4.14 (br s), 4.13–4.08 (br s), 4.02–3.95 (br s), 3.90–3.82 (br), 3.72–3.66 (s), 3.54–3.46 (br s), 3.44 3.13 (quint), 2.89–2.77 (s), 2.69–2.59 (s), 2.58–2.53 (s), 2.48–2.36 (s), 2.32–2.27 (br s), 2.25–2.21 (br s), 2.20–2.15 (br), 2.15–2.11 (br s), 2.11–2.09 (br s), 2.05–2.03 (br s), 2.00–1.94 (s), 1.92–1.87 (br s), 1.86–1.77 (br), 1.35–1.32 (br d), 1.26–1.24 (br s), 1.23–1.19 (br s); **12**: δ 7.88–7.49 (br s), 5.65–5.52 (br s), 5.44–5.35 (br s), 5.31–5.21 (br s), 5.02–4.97 (br s), 4.95–4.91 (br), 4.89–4.88 (br d), 4.85–4.84 (br d), 4.81–4.79 (d), 4.74–4.71 (br s), 4.68–4.61 (br), 4.48–4.35 (br s), 4.35–4.23 (br s), 4.23–4.13(br s), 4.13–4.03 (br s), 4.02–3.93 (br s), 3.90–3.80 (br s), 3.73–3.63 (s), 3.55–3.45 (br s), 3.40–3.14 (t), 2.91–2.71 (s), 2.71–2.58 (s), 2.58–2.51 (s), 2.51–2.31 (s), 2.31–2.26 (br s), 2.26–2.21 (br s), 2.21–2.12 (br s), 2.05–2.02 (br s), 2.00–1.94 (s),1.93–1.88 (br s), 1.85–1.78 (br s), 1.35–1.32 (br d), 1.26–1.23 (br s). HPLC: **10** (t_r = 9.06 min; purity = 99%); **11** (t_r = 9.45 min; purity = 99%); **12** (t_r = 9.68 min; purity = 99%).

Isothermal Titration Calorimetry. All experiments were carried out using a Nano ITC Standard Volume from TA Instruments (Lindon, UT). Binding conditions were optimized for each dendrimer conjugate. Experiments were all performed in PBS buffer (pH 7.4). Buffer was degassed prior to an experiment for 25 min at room temperature with a stir rate of 610 rpm. In a multiple injection mode, the experiment was set up using the following parameters: 25 °C, 250 rpm, 500–700 s between injections, 20 injections of 10 μL each. Upon filling the cell and syringe, stirring was turned on and allowed to equilibrate for ∼1 h. Experiment was initiated when the baseline power difference was <0.4 μW within 5 min. Control experiments were performed with the injection of the dendrimer conjugates into the PBS buffer. All data were recorded with the TA Instruments software provided. Further analysis was performed using TA NanoAnalyze Version 2.1.13. The area under each peak was integrated, and the resulting data were modeled using an independent model fit with the three variables, n, ΔH, and K_A. Using the fit output of ΔH and K_A, ΔG and ΔS were determined at 25 °C. Statistics were then performed on the thermodynamic parameters with a desired confidence interval of 95%. Each experiment was repeated 2–8 times, and the average from multiple runs was used to obtain K_D (= $1/K_A$).

Differential Scanning Calorimetry. DSC measurements were performed using a Nano DSC from TA Instruments (Lindon, UT). Experiments were performed in 10 mM phosphate buffer, pH 7.0. Buffer was degassed prior to each experiment for 25 min at room temperature with a stir rate of 610 rpm. The sample and reference were allowed to equilibrate for ∼30 min until stabilization was achieved. Experiment was initiated when the baseline power difference

remained within a tenth of a microwatt over 5 min. All experiments were performed at 3 atm pressure. For all scans, the low-temperature limit was 25 °C and the high temperature limit was 100 °C. The scan rate was 1.0 °C/min. Scans of the buffer as sample and reference were measured to determine a baseline. All data were recorded with the TA Instruments software. To obtain molar heat capacity (MHC) data, the baseline was subtracted and further analysis was performed using TA NanoAnalyze Version 2.1.13. Additional calculations used by the program included inputs on the concentration, molecular mass of the bound complex, and the apparatus cell volume (0.3 mL). The molar mass of RfBP was taken as 30 kDa, and the concentration used in all measurements was 1 mg/mL. Analysis was performed using a two-state scaled model.

RESULTS AND DISCUSSION

Synthesis of RF-Conjugated PAMAM Dendrimers. The delivery platform used for this study is based on a G5 poly(amidoamine) (PAMAM) dendrimer (diameter 5.4 nm).[27,38] This dendrimer particle has a large number of primary amines (theoretically 128), each branched repetitively on its periphery, and each of the amine branches is available for covalent conjugation with a variety of targeting ligands, making the dendrimer an excellent system for the multivalent ligand design.[31,39−41] We approached the design of RF-presenting G5 dendrimer conjugates by evaluating two key design factors (Figure 1): (1) variation of the ligand orientation by presenting the ligand attached at its N-3 and N-10 position and (2) variation of the ligand valency (the number of the ligands attached per dendrimer). First, we designed a series of G5-N(3)-RF$_n$ conjugates **4**−**7** (Scheme 1) in which each dendrimer contains the RF ligand tethered at the N-3 position and at a variable average valency (n = 0, 2.8, 4.5, and 11.1). This conjugate series was prepared by the amide coupling of the G5 PAMAM dendrimer with 3-carboxymethylriboflavin (**1**)[36,37] added at variable molar equivalents to the dendrimer. Synthesis of the conjugate series was performed by an EDC-based method involving two reactions performed in a sequence (step i, ii), where **1** was preactivated to its NHS ester **2** prior to the reaction with the dendrimer. After this coupling step, each of the unreacted surface amines was converted to *N*-acetyl amide, making the dendrimer surface neutral. In this sequential approach, we controlled the molar ratio between **1** and the dendrimer G5-$(NH_2)_{110}$ and were able to prepare those RF conjugates **3**−**6**. The conjugate **7** contains a fluorescent dye (FITC), an imaging molecule commonly employed for cell uptake studies. It was introduced to determine if the presence of the dye molecule itself makes an impact on the binding affinity of the RF ligand indirectly through a steric effect. This dye-containing RF dendrimer was prepared through an additional coupling step (iii) for the FITC prior to the final exhaustive N-acetylation.

Scheme 1. Synthesis of PAMAM Dendrimers 3−7, Each Conjugated with the RF Ligand at the N-3 position[a]

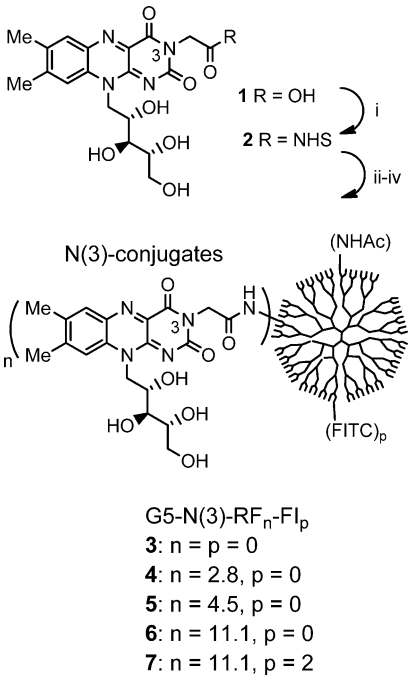

[a]Reagents and conditions: (i) *N*-hydroxysuccinimide, dimethylaminopyridine (DMAP), EDC, DMF, rt, 12 h; (ii) 2 added in variable mol. equiv to G5 PAMAM dendrimer G5-$(NH_2)_{110}$, MeOH, rt, 3 days; (iii) fluorescein isothiocyanate (FITC; added for conjugate 7 only), rt, 24 h; and (iv) excess Ac_2O, Et_3N, 6 h, rt.

Each RF conjugate was purified by exhaustive dialysis using a membrane tubing (MWCO 10 kDa), and its purity was in the range of 95−98%, as determined by the anal. HPLC method in which the AUC (area under curve at 285 nm) value for each RF-conjugated dendrimer was compared with that of free RF or RF ligand (Figure S3 of the Supporting Information). The molecular mass of the conjugate was measured by the MALDI mass spectral analysis (m/z, g mol^{-1}): **4** (33 400); **5** (35 300); **6** (36 900); **7** (38 200) (Figure S1 of the Supporting Information). Each RF conjugate was fully characterized by employing other relevant analytical techniques including ^{1}H NMR spectroscopy (Figure 2a, Figure S2 of the Supporting Information) and UV/vis spectrometry (Figure 2b, Figure S4 of the Supporting Information). Selected spectral data for the new conjugates **4**−**7** are shown in Figure 2. These data provide evidence of the tethering of the RF ligand to the dendrimer, as suggested by RF-specific aromatic protons in the ^{1}H NMR spectra (broad peaks at 7.6 to 8.4 ppm) and by the strong absorption at longer wavelengths that points to the isoalloxazine chromophore (λ_{max} = 449 nm; ε = 12 100 M^{-1} cm^{-1}). The number of RF ligands attached to each dendrimer conjugate was determined on a mean basis by the analysis of the ^{1}H NMR, UV/vis, and MALDI mass spectral data, as summarized in Table S1 of the Supporting Information. The valency of RF ligands that is referred for each dendrimer conjugate in this article is, however, based on the ^{1}H NMR analysis because of its greater accuracy.[42,43] The efficiency for ligand conjugation (no. RF ligand conjugated per dendrimer relative to no. RF ligand added) was approximately 40−50% for this series of the conjugates (**4** to **7**). Such efficiency is acceptable but lower than that observed frequently in the amide conjugation of small molecules (>80%). We believe that a number of factors might be responsible such as steric congestion on the dendrimer surface[34] and decreased reactivity of dendritic branches due to backfolding.[26,27]

Second, we designed another series of RF-presenting dendrimer conjugates G5-RF(10)-RF$_m$ **10**−**12** (Scheme 2) in which each RF ligand is attached to the dendrimer through a glutaric acid spacer linked at its N-10 position. To attach the RF to the spacer, we synthesized a glutaryl derivative of RF **8** (HRMS-ESI, negative ion mode: calcd for $C_{22}H_{26}N_4O_9$ [M-H]$^-$, m/z = 489.1627, found 489.1620), a covalent adduct formed by an ester linkage at its hydroxyl group of the (D)-

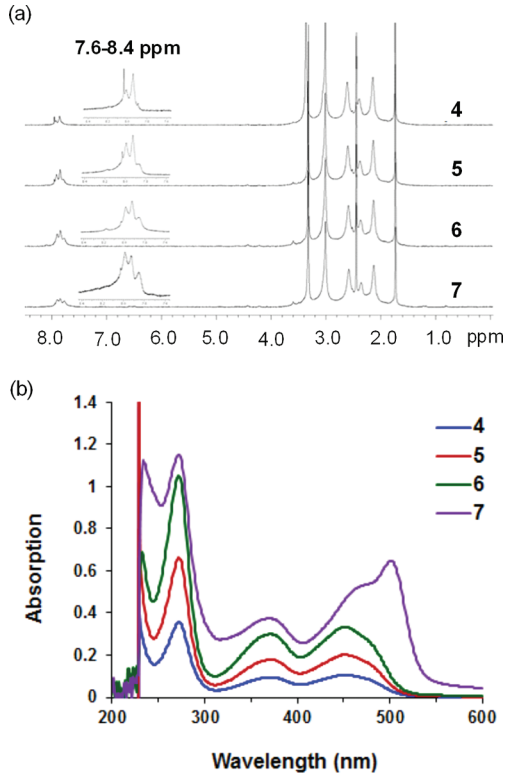

Figure 2. (a) ^{1}H NMR spectra of RF-conjugated dendrimers G5-N(3)-RF$_n$ **4**–**7** and (b) their UV/vis spectra, each measured at 0.1 mg/mL concentration in PBS (pH 7.4).

ribose unit. A number of similar RF conjugation reactions have been previously reported elsewhere,[29,30,44] each suggesting that the coupling reaction might occur regioselectively at the primary hydroxyl group, perhaps because it is more sterically favored than those secondary alcohols located adjacent to the bulky isoalloxazine head. Synthesis of this N-10 conjugate series **10**–**12** was performed similarly, as previously illustrated by an EDC-based coupling method (step ii, iii), followed by the exhaustive *N*-acetylation of remaining primary amines.

Each conjugate in this series was purified by the dialysis method as previously described, and its purity was 99%, as determined by the anal. HPLC method (Figure S3 of the Supporting Information). Each RF conjugate was fully characterized by ^{1}H NMR spectroscopy, UV/vis, and MALDI mass spectrometry (m/z, g mol^{-1}): **10** (33 700); **11** (36 900); and **12** (40 300). Ligand valency for each dendrimer conjugate was determined on a mean basis by the analysis of the ^{1}H NMR, UV/vis, and MALDI mass spectral data, as summarized in Table S1 of the Supporting Information.

Distribution of RF Ligands. The amide conjugation reaction applied for the attachment of RF ligands to the G5 PAMAM dendrimer occurs in a stochastic fashion and generates a distribution of the numbers of ligands conjugated per dendrimer.[42,43] Figure 3 illustrates the Poissonian distribution of the ligand-conjugated dendrimers simulated for the three dendrimer conjugates, each having a mean number of 2.8, 4.5, and 11.1 ligands. For example, **4** G5-N(3)-RF$_n$ (n = 2.8) is experimentally determined to have approximately three RF ligands attached per dendrimer on an average basis. The stochastic reaction conditions result in a multivalent dendrimer species ($n \approx 0$–8; median ≈ 4) with the highest population at n = 2. Therefore, it is noted that the thermodynamic parameters

Scheme 2. Synthesis of PAMAM Dendrimers 10–12, Each Conjugated with RF at N10 Position[a]

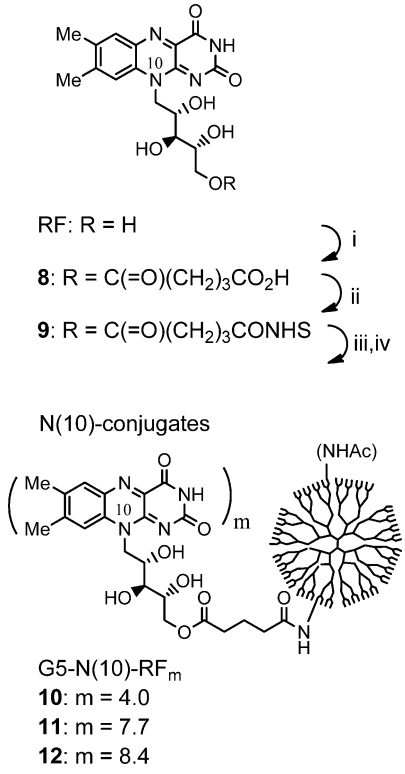

[a]Reagents and conditions: (i) glutaric anhydride, pyridine, DMSO, 90 °C, 12 h; (ii) *N*-hydroxysuccinimide, dimethylaminopyridine (DMAP), EDC, DMF, rt, 16 h; (iii) **9** added in variable mol. equiv to G5 PAMAM dendrimer G5-$(NH_2)_{110}$, MeOH, rt, 2 d; and (iv) excess Ac_2O, Et_3N, 6 h, rt.

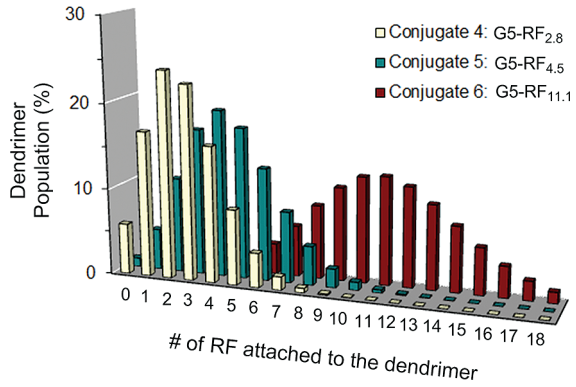

Figure 3. Theoretical distribution of RF ligands attached per dendrimer acquired by Poissonian simulation. Each of the RF-conjugated dendrimer conjugates G5-N(3)-RF$_n$ **4**–**6** has the mean value of 2.8, 4.5, or 11.1 RF ligands per dendrimer.

we studied here for the effect of the ligand valency are understood on a mean basis.

Thermodynamic Measurements. We first used ITC to characterize the thermodynamic response of the dendrimer-RF conjugate to the RfBP. In our previous study of "free" RF ligand binding to RfBP, we determined the binding stoichiometry (n) from ITC to be 1:1, which has also been confirmed by fluorescence quenching studies.[45,46] However, with the RF conjugated dendrimers, we observe that not all RF sites on the dendrimer are occupied by RfBP. (See Tables 1 and 2.) On the

dx.doi.org/10.1021/bm201566g | *Biomacromolecules* 2012, 13, 507–516

Table 1. Thermodynamic Parameters for the Binding of N-3 RF Dendrimer Conjugates with RfBP in PBS (pH 7.4) at 25°C

system (vs RfBP)	n^a	K_d (nM)^b	ΔH^a (kJ mol^{-1})	ΔG (kJ mol^{-1})	$-T\Delta S$ (kJ mol^{-1})
3, G5-$(RF)_0$	NB	NB	NB	NB	NB
4, G5-$(RF)_{2.8}$	1.76 ± 0.06	465 ± 12	−41.0 ± 2.7	−36.2	4.8
5, G5-$(RF)_{4.5}$	1.24 ± 0.06	568 ± 95	−55.7 ± 3.8	−35.3	20.4
6, G5-$(RF)_{11.1}$	1.63 ± 0.14	1170 ± 90	−46.5 ± 5.3	−33.7	12.8
7, G5-$(RF)_{11.1}$-$(FI)_2$	5.11 ± 0.51	2075 ± 243	−13.0 ± 2.7	−32.2	−19.2

^{a}Reported errors are from fitting data. ^{b}Reported errors are from averaging multiple runs. NB: no binding.

Table 2. Thermodynamic Parameters for the Binding of N-10 RF Dendrimer Conjugates with RfBP in PBS (pH 7.4) at 25°C

system (vs RfBP)	n^a	K_d (nM)^b	ΔH^a (kJ mol^{-1})	ΔG (kJ mol^{-1})	$-T\Delta S$ (kJ mol^{-1})
10, G5-$(RF)_{4.0}$	2.88 ± 0.27	2671 ± 199	−15.7 ± 2.3	−31.9	−16.3
11, G5-$(RF)_{7.7}$	5.16 ± 0.76	4049 ± 13	−9.0 ± 2.2	−30.8	−21.8
12, G5-$(RF)_{8.4}$	2.94 ± 0.77	5551 ± 1064	−13.3 ± 6.1	−30.0	−16.7

^{a}Reported errors are from fitting data. ^{b}Reported errors are from averaging multiple runs.

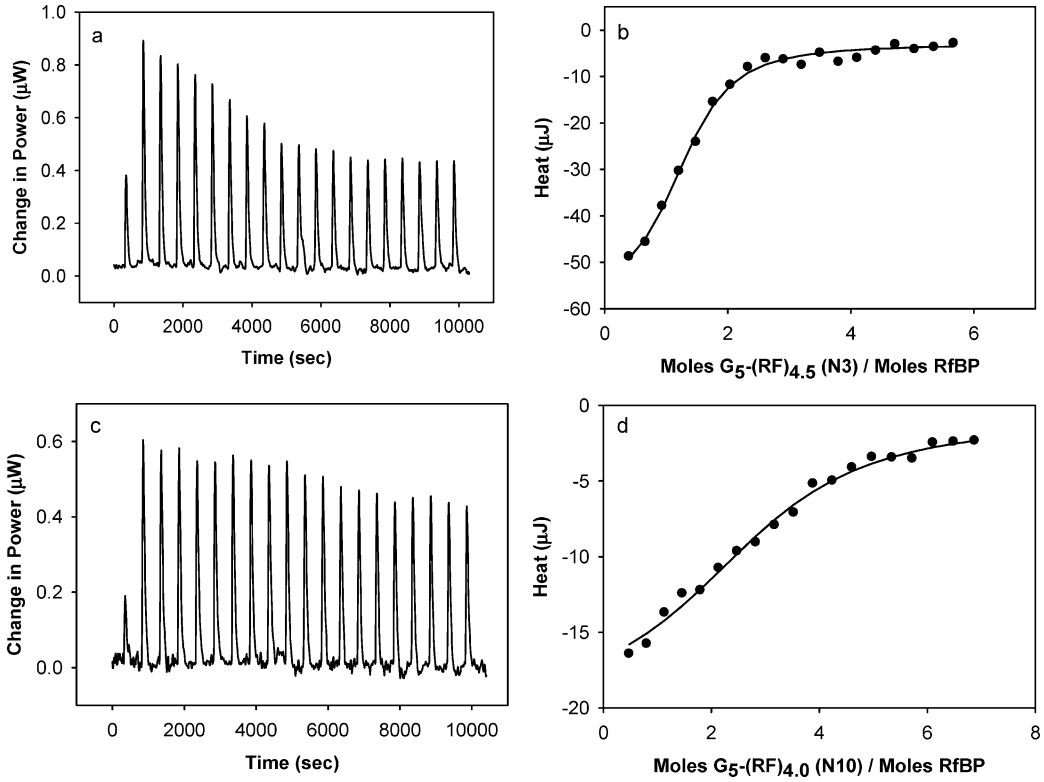

Figure 4. Raw ITC data for the interaction between (a) G5-$(RF)_{4.5}$ at the N-3 position and (c) G5-$(RF)_{4.0}$ at the N-10 position with chicken RfBP (4 μM) at 25 °C in PBS buffer. Plot of integrated area under each injection peak for G5-$(RF)_{4.5}$ at the N-3 position (b) and G5-$(RF)_{4.0}$ at the N-10 position (d). The solid line (b and d) is an independent model fit to data with parameters n, K_A, and ΔH.

basis of a simple sphere model where the dendrimer molecule ($d \approx 6$ nm) and the protein molecule ($d \approx 4$ to 5 nm) are treated as two interacting spheres, approximately 6 to 7 RfBPs can be theoretically accommodated around the RF-conjugated dendrimer particle. This analysis is in close agreement with the maximal number ($n \approx 5$; Tables 1 and 2) we obtained from ITC measurements. Four dendrimer conjugates tethered at the N-3 position of RF with an average RF valency of 0, 2.8, 4.5, or 11.1 were screened for determining their binding affinities to RfBP (conjugates **3**−**6**; Table 1). We also screened an additional conjugate **7**, which has an average of 11.1 RFs linked at the N-3 position and contains an average number of two fluorescein dye molecules as well. Three dendrimer conjugates tethered at the N-10 position, which provides more flexibility via the longer glutarate linker installed at the ribose terminus of RF were screened, with an average RF valency of 4.0, 7.7, or 8.4 (conjugates **10**−**12**; Table 2). A representative ITC curve is shown in Figure 4 for the binding of G5-$(RF)_{n(=\ 4\ or\ 4.5)}$ with RfBP at the N-3 position (Figure 4a,b) and the N-10 position (Figure 4c,d). Thermodynamic data for the binding of RF-dendrimer conjugates to RfBP for the series at N-3 and N-10 are shown in Tables 1 and 2.

In comparison with the "free" RF binding to RfBP (K_D = 5 nM),[16] the dissociation constant, K_D for all dendrimer conjugates screened is a factor of 93−1110 times greater. This implies that the binding affinity of the dendrimer-conjugated RF ligand to RfBP is significantly decreased. Furthermore, the K_D values in Tables 1 and 2 highlight the

fact that the N-3-bound dendrimer series has an overall higher affinity to RfBP in comparison with the RF-dendrimer conjugates tethered at the N-10 position. Comparison of two orthogonal conjugates **5** and **10**, each having a similar average number of RFs bound to the dendrimer but otherwise RF attached at a different position N-3 or N-10, shows a factor of ~5× greater K_D value at the latter position. It clearly signifies that contacts made in the binding pocket by the RF molecule with a free ribose moiety are important and thus could lead to tighter binding in the binding pocket. The magnitude of change in free energy for the N-3 and N-10 series is comparable and shows only a slight increase in free energy with increasing RF valency for each series. To gain insight into the large differences in affinity of the N-3 and N-10 RF-dendrimer conjugates to RfBP, the enthalpic (ΔH) and the entropic ($-T\Delta S$) contributions were examined and are shown in Figure 5. A typical enthalpy−entropy compensation plot is also shown in

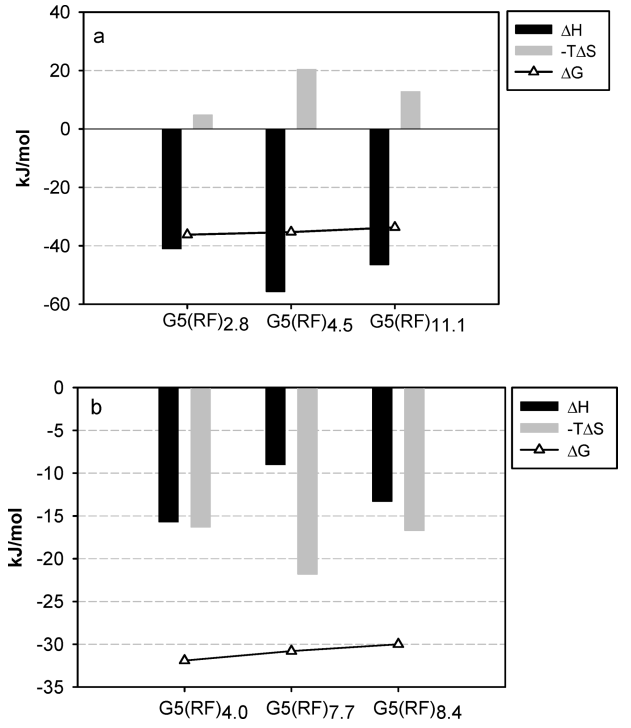

Figure 5. Thermodynamic parameters, including $-T\Delta S$, ΔH, and ΔG representing the association of N-3 (a) and N-10 (b) RF dendrimer conjugates with RfBP and with increasing valency of RF.

Figure 6 for both the N-3 and N-10 dendrimer conjugates, and a strong linear correlation between the entropic and enthalpic terms of the Gibbs equation is noted.[47] For the N-3 dendrimer conjugates, the enthalpy change is favorable, and the dendrimer with an RF valency of 4.5 is the most favorable of the ligand valencies examined (Table 1). By contrast, the entropic penalty ($-T\Delta S$) increased from 4.8 to 20.4 kJ/mol for the N-3 RF dendrimer conjugates with the highest entropic penalty observed for the dendrimer with a valency of 4.5. This implies that the binding of the N-3 series of RF dendrimer conjugates is largely enthalpy driven, whereas the addition of RF units per dendrimer results in an entropic penalty most likely due to steric hindrance[34,48] or repulsions arising from having RF molecules in close proximity to the dendrimer. In addition to using a dendrimer platform for targeted delivery of drug conjugates, imaging molecules could also be attached to the

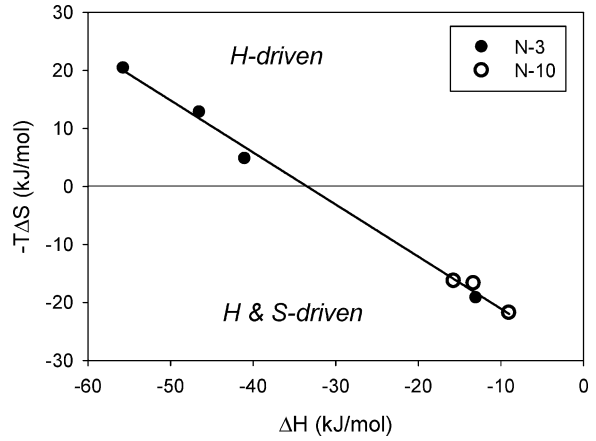

Figure 6. $-T\Delta S$ versus ΔH (kJ/mol) scatter plot for the binding of RF−dendrimer conjugates at N-3 and N-10 positions to RfBP at 25 °C. The linear regression is given by $-T\Delta S$ (kJ·mol^{-1}) = (−0.90 ± 0.03) ΔH (kJ·mol^{-1}) − 30.0 ± 0.9 kJ·mol^{-1} (R^2 = 0.9955, P < 0.0001).

dendrimer to verify the delivery of the payload. As such, we also examined the binding of an N-3 dendrimer conjugate **7**, which included an average of 11.1 RFs and 2 FITC molecules. In the latter case, the dissociation constant (K_D) increased nearly two-fold in comparison with an equivalent N-3 dendrimer conjugate **6**, which included only an average of 11.1 RFs. This decrease in affinity was accompanied by significant changes in both enthalpy and entropy. An enthalpic penalty of 33.5 kJ/mol and the entropic favorability for **7** relative to **6** highlights in this case that the binding is enthalpy−entropy-driven. (See Figure 6.) These dramatic changes in both entropic and enthalpic factors suggest that the mode of binding may have changed due to the presence of the imaging molecule. Structurally both FITC and RF are similar in that each contains three fused aromatic rings, whereas the hydrophilic ribose moiety of the RF is replaced by a hydrophobic moiety in FITC. The latter may account for the significant changes in both entropic and enthalpic factors. In contrast with the N-3 series, the binding of N-10 dendrimer conjugates to RfBP shows an enthalpic penalty, where the enthalpy is nearly a factor of 4−6 times smaller in comparison with the N-3 dendrimer conjugates (Table 2). However, the N-10 series of dendrimer conjugates show a favorable entropic effect upon binding to RfBP in comparison with the unfavorable entropic effects observed for the N-3 series (Figure 5b). The enthalpic penalty observed for the N-10 series of dendrimer conjugates is most likely due to the desolvation of the ribose hydroxyl groups upon complexation with RfBP and the resulting release of water molecules leading to an entropic gain.[49] The binding affinity, however, decreased by nearly a factor of 5 for the N-10 series, suggesting that the enthalpy of interaction in the binding pocket between the RF-dendrimer and the RfBP was not able to overcome the enthalpic penalty arising from the desolvation of the polar groups of the ribose moiety.[49] This further implies that the RF molecules bound at the N-10 position to the dendrimer lack the optimal geometry required for binding to RfBP. Finally, as in the N-3 series, the N-10 series of dendrimer conjugates also show an increase in K_D with increasing RF valency, suggesting steric hindrance or repulsions between RF groups, due to overcrowding on the dendrimer are likely to lead to a decrease in affinity.[34] In summary, the ITC study suggests that: (i) the N-3 position of RF is a preferred position for the dendrimer conjugation and (ii) presentation of targeting ligands at too

high valency such as n = 11 could prevent from achieving an optimal affinity for individual RF ligands involved in the receptor binding.

Because RF binding to RfBP is known to cause protein structure stabilization,[50,51] a DSC study was performed with four RF conjugates **3**, **5**−**7** to investigate the extent of structural stability of RfBP upon binding to dendrimer−RF conjugates. The DSC thermograms were also acquired for three other RF−dendrimer conjugates **10**−**12** linked at the N-10 position, which included those with an average of 4.0, 7.7, and 8.4 RF molecules. Figure 7 demonstrates the effect on protein stability of N-3 and N-10 conjugated dendrimers with an RF valency of

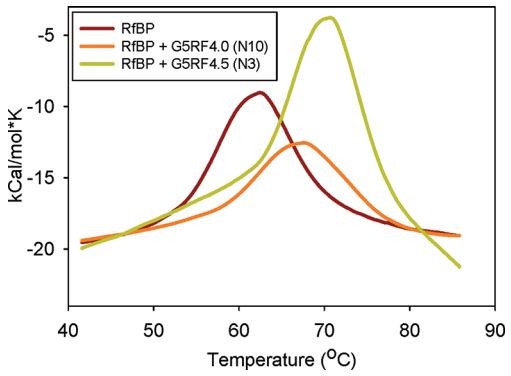

Figure 7. Changes in denaturation temperature as a result of ligand binding: apo RfBP; RfBP in complex with conjugate **10**, G5-$(RF)_{4.0}$ linked at the N-10 position; RfBP in complex with conjugate **5**, and G5-$(RF)_{4.5}$ linked at the N-3 position. Protein concentration was 1 mg/mL in 10 mM phosphate buffer, pH 7.0. Scan rate was 1.0 °C min^{-1} with temperature range 25−100 °C.

4.5 and 4.0, respectively. Apo-RfBP undergoes a reversible endothermic transition with a maximum denaturation temperature (T_m) at 62.1 °C and is in close agreement with the 61.06 °C (T_m) obtained in previous DSC studies.[52] Upon binding to RfBP, the maximum of denaturation temperature of the RfBP shifted to 67.8 °C for the conjugate **10**, G5-$(RF)_{4.0}$ N-10, and to 70.5 °C for the conjugate **5**, G5-$(RF)_{4.5}$ N-3 (Figure 7). The transition maximum for RfBP with a control conjugate **3**, G5-$(RF)_0$, was 62.3 °C. These results demonstrate that the shift in T_m observed is only due to the binding of RF-dendrimer conjugates to the RfBP. The increase in denaturation temperature of RfBP is dependent on the RF linker site: 5.7 °C for G5-$(RF)_{4.0}$ N-10 and 8.4 °C for G5-$(RF)_{4.5}$ N-3. These DSC data correspond well with ITC data that suggest that the binding affinity to RfBP is determined by how RF ligands are linked to the dendrimer. Therefore, according to the ITC study, the conjugate **5** with RF linked at the N-3 position showed greater affinity than the conjugate **10**, and the DSC study showed that greater stability was achieved by the conjugate **5** with a T_m of 70.5 °C and an unfolding enthalpy of 101.9 kcal/mol (Table 3). In comparison, the protein−ligand complex formed between RfBP and free RF shows a T_m of 72.8 °C and an unfolding enthalpy of 114.8 kcal/mol.[51,52] Additionally, the DSC data show that varying the valency of the RF molecules on the dendrimer affects protein stability. As the average valency of RF molecules attached to the dendrimer at N-3 increases from 4.5 to 11.1 the transition maximum of RfBP decreases from 70.5 to 67.4 °C, whereas the enthalpy for unfolding decreases from 101.9 to 85.3 kcal/mol. (See Table 3.) This clearly suggests that the G5-$RF_{4.5}$ is more tightly bound to the RfBP

Table 3. Shifts in Thermal Denaturation[ab]

	T_m [°C]	ΔH [kcal mol^{-1}]	standard deviation around fit
RfBP	62.1	84.2	0.11
RfBP+G5-$(RF)_0$ **3**	62.3	80.0	0.10
N-3			
RfBP+G5-$(RF)_{4.5}$ **5**	70.5	101.9	0.14
RfBP+G5-$(RF)_{11.1}$ **6**	69.7	91.0	0.17
RfBP+G5-$(RF)_{11.1}$-$(FI)_2$ 7	67.4	85.3	0.19
N-10			
RfBP+G5-$(RF)_{4.0}$ **10**	67.8	72.6	0.07
RfBP+G5-$(RF)_{7.7}$ **11**	66.4	72.6	0.09
RfBP+G5-$(RF)_{8.4}$ **12**	65.6	65.6	0.07

[a]DSC experiments were performed in 10 mM phosphate buffer, pH 7.0. [b]Protein concentration was 1 mg/mL. Dendrimer conjugate concentration was 140−325 uM.

than G5-$RF_{11.1}$, a result also confirmed by ITC. Similarly, the N-10 RF conjugated dendrimers show a decrease in RfBP transition maximum from 67.8 to 65.6 °C with increasing RF valency. However, a smaller enthalpy decrease is observed in comparison with the N-3 bound dendrimers. Furthermore, the enthalpy for unfolding with the N-10 dendrimer conjugates is lower than the enthalpy of the apo-RfBP. Because the T_m values for the N-10 dendrimer conjugates are higher than the T_m value for apo-RfBP, enthalpy alone cannot explain the changes observed here. The DSC data in combination with the ITC results for the N-10 dendrimer conjugates demonstrate that entropic factors play a key role in the binding of these RF-dendrimer conjugates to RfBP. The decrease in T_m as the number of RF molecules on the dendrimer is increased (for both N-3 and N-10) corresponds well with ITC results, which indicate that increasing the valency of RFs attached to the dendrimer results in decreased binding strength. This negative correlation of valency with the affinity constant might be due to unfavorable constraints such as steric congestion[34] that occurs as more bulky receptors are recruited to the dendrimer surface.

In analyzing the receptor−ligand interactions from ITC and DSC, we assume that all ligands attached to a single dendrimer nanoparticle would have equivalent K_D values. This is because such binding affinities are determined from binding to free RfBPs and in a manner independent of any of the constraints that would occur if the identical dendrimer-linked RF ligands bind to multiple RfBPs on a cell surface.[7] However, in a cell-based receptor system, individual ligands attached to a single dendrimer nanoparticle might have different K_D values because RfBPs are restricted in their location and lateral movement on the cell surface.

CONCLUSIONS

In conclusion, we have examined two new series of dendrimers, each conjugated with RF ligands attached at the isoalloxazine site (N-3) or the D-ribose site at (N-10) and with varying average ligand valency. The binding of these RF−dendrimer conjugates with RfBP were performed by ITC and DSC. The K_D values measured by ITC show that the RF ligand conjugated to the dendrimer has an affinity much lower than that of free RF toward the RfBP. Furthermore, the binding affinity was found to decrease with increasing valency of RF on the dendrimers. Of the two conjugate series, the RF linked at the N-3 position showed greater affinity toward RfBP. These results were independently confirmed by DSC, where greater

protein−conjugate stability was achieved with the N-3 series and at a lower ligand valency. In summary, the current biophysical studies provide direct information on the strength of discrete monovalent interactions that might constitute the multivalent interaction. These studies should be complementary to cell-based avidity assays that investigate the targeting capability of multivalent ligands based on a multivalent binding.[3−6] These results demonstrate the need to understand and better design an optimized geometry for RF−dendrimer conjugates to be used in targeted drug delivery.

■ ASSOCIATED CONTENT

Ⓢ Supporting Information

Experimental details and additional characterization data (MALDI-TOF mass spectra, ^{1}H NMR spectra, UV/vis spectra, and anal. HPLC traces) are provided online. This material is available free of charge via the Internet at http://pubs.acs.org.

■ AUTHOR INFORMATION

Corresponding Author

*Phone: (734) 615-0618; Fax: (734) 615-0621; E-mail: skchoi@umich.edu (S.K.C.). Phone: (616) 526-6058; Fax: (616) 526-6501; E-mail: ksinniah@calvin.edu (K.S.). Phone: (734) 647-2777; Fax: (734) 936-2990; E-mail: jbakerjr@umich.edu (J.R.B.).

■ ACKNOWLEDGMENTS

K.S. acknowledges the support of NSF (CHE-0959681) and HHMI (student support). Part of this work was supported by NCI, NIH under award 1 R01 CA119409 (J.R.B.).

■ REFERENCES

(1) Hong, S.; Leroueil, P. R.; Majoros, I. J.; Orr, B. G.; Baker, J. R. Jr.; Banaszak Holl, M. M. *Chem. Biol.* **2007**, *14*, 107−115.
(2) Montet, X.; Funovics, M.; Montet-Abou, K.; Weissleder, R.; Josephson, L. *J. Med. Chem.* **2006**, *49*, 6087−6093.
(3) Mammen, M.; Choi, S. K.; Whitesides, G. M. *Angew. Chem., Int. Ed.* **1998**, *37*, 2754−2794.
(4) Kiessling, L. L.; Gestwicki, J. E.; Strong, L. E. *Curr. Opin. Chem. Biol.* **2000**, *4*, 696−703.
(5) Lee, Y. C.; Lee, R. T. *Acc. Chem. Res.* **1995**, *28*, 321−327.
(6) Roy, R. *Curr. Opin. Struct. Biol.* **1996**, *6*, 692−702.
(7) Thomas, T. P.; Choi, S. K.; Li, M.-H.; Kotlyar, A.; Baker, J. R. Jr. *Bioorg. Med. Chem. Lett.* **2010**, *20*, 5191−5194.
(8) Kukowska-Latallo, J. F.; Candido, K. A.; Cao, Z.; Nigavekar, S. S.; Majoros, I. J.; Thomas, T. P.; Balogh, L. P.; Khan, M. K.; Baker, J. R. Jr. *Cancer Res.* **2005**, *65*, 5317−5324.
(9) Low, P. S.; Henne, W. A.; Doorneweerd, D. D. *Acc. Chem. Res.* **2008**, *41*, 120−129.
(10) Myc, A.; Majoros, I. J.; Thomas, T. P.; Baker, J. R. Jr. *Biomacromolecules* **2007**, *8*, 13−18.
(11) Pan, X.; Lee, R. J. *Expert Opin. Drug Delivery* **2004**, *1*, 7−17.
(12) Majoros, I. J.; Williams, C. R.; Baker, J. Jr. *Curr. Top. Med. Chem.* **2008**, *8*, 1165−1179.
(13) Majoros, I. J.; Williams, C. R.; Becker, A.; Baker, J. R. Jr. *Wiley Interdiscip. Rev.: Nanomed. Nanobiotechnol.* **2009**, *1*, 502−510.
(14) Hilgenbrink, A. R.; Low, P. S. *J. Pharm. Sci.* **2005**, *94*, 2135−2146.
(15) Lee, R. J.; Low, P. S. *Biochim. Biophys. Acta, Biomembr.* **1995**, *1233*, 134−144.
(16) Plantinga, A.; Witte, A.; Li, M.-H.; Harmon, A.; Choi, S. K.; Banaszak Holl, M. M.; Orr, B. G.; Baker, J. R. Jr; Sinniah, K. *ACS Med. Chem. Lett.* **2011**, *2*, 363−367.
(17) Shukla, R.; Thomas, T. P.; Peters, J.; Kotlyar, A.; Myc, A.; Baker, J. R. Jr. *Chem. Commun.* **2005**, 5739−5741.
(18) Temming, K.; Lacombe, M.; Schaapveld, R. Q. J.; Orfi, L.; Kéri, G.; Poelstra, K.; Molema, G.; Kok, R. J. *ChemMedChem* **2006**, *1*, 1200−1203.
(19) Chen, Y.; Foss, C. A.; Byun, Y.; Nimmagadda, S.; Pullambhatla, M.; Fox, J. J.; Castanares, M.; Lupold, S. E.; Babich, J. W.; Mease, R. C.; Pomper, M. G. *J. Med. Chem.* **2008**, *51*, 7933−7943.
(20) Shukla, R.; Thomas, T. P.; Desai, A. M.; Kotlyar, A.; Park, S. J.; Baker, J. R. Jr *Nanotechnology* **2008**, *19*, 295102.
(21) Qian, Z. M.; Li, H.; Sun, H.; Ho, K. *Pharmacol. Rev.* **2002**, *54*, 561−587.
(22) Thomas, T. P.; Shukla, R.; Kotlyar, A.; Liang, B.; Ye, J. Y.; Norris, T. B.; Baker, J. R. Jr *Biomacromolecules* **2008**, *9*, 603−609.
(23) Raha, S.; Paunesku, T.; Woloschak, G. *Wiley Interdiscip. Rev.: Nanomed. Nanobiotechnol.* **2010**, 269−281.
(24) Karande, A. A.; Sridhar, L.; Gopinath, K. S.; Adiga, P. R. *Int. J. Cancer* **2001**, *95*, 277−281.
(25) Johnson, T.; Ouhtit, A.; Gaur, R.; Fernando, A.; Schwarzenberger, P.; Su, J.; Ismail, M. F.; El-Sayyad, H. I.; Karande, A.; Elmageed, Z. A.; Rao, P.; Raj, M. *Front. Biosci.* **2009**, *14*, 3634−3640.
(26) Tomalia, D. A.; Baker, H.; Dewald, J.; Hall, M.; Kallos, G.; Martin, S.; Roeck, J.; Ryder, J.; Smith, P. *Polym. J.* **1985**, *17*, 117−132.
(27) Tomalia, D. A.; Naylor, A. M.; William, A.; Goddard, I. *Angew. Chem., Int. Ed.* **1990**, *29*, 138−175.
(28) Monaco, H. L. *EMBO J.* **1997**, *16*, 1475−1483.
(29) Huang, S.-N.; Phelps, M. A.; Swaan, P. W. *J. Pharmacol. Exp. Ther.* **2003**, *306*, 681−687.
(30) Holladay, S. R.; Yang, Z.-f.; Kennedy, M. D.; Leamon, C. P.; Lee, R. J.; Jayamani, M.; Mason, T.; Low, P. S. *Biochim. Biophys. Acta, Gen. Subj.* **1999**, *1426*, 195−204.
(31) *Dendrimer-Based Nanomedicine*; Majoros, I., Baker, J. R., Jr, Eds.; Pan Stanford: Singapore, 2008.
(32) Choi, Y.; Thomas, T.; Kotlyar, A.; Islam, M. T.; Baker, J. R. Jr. *Chem. Biol.* **2005**, *12*, 35−43.
(33) Lu, Y.; Low, P. S. *Adv. Drug Delivery Rev.* **2002**, *54*, 675−693.
(34) Choi, S. K.; Leroueil, P.; Li, M.-H.; Desai, A.; Zong, H.; Van Der Spek, A. F. L.; Baker, J. R. Jr. *Macromolecules* **2011**, *44*, 4026−4029.
(35) Choi, S. K.; Thomas, T.; Li, M.; Kotlyar, A.; Desai, A.; Baker, J. R. Jr. *Chem. Commun.* **2010**, *46*, 2632−2634.
(36) Caelen, I.; Kalman, A.; Wahlstrom, L. *Anal. Chem.* **2003**, *76*, 137−143.
(37) Wu, F. Y. H.; MacKenzie, R. E.; McCormick, D. B. *Biochemistry* **1970**, *9*, 2219−2224.
(38) Liang, C.; Fréchet, J. M. J. *Prog. Polym. Sci.* **2005**, *30*, 385−402.
(39) Cloninger, M. J. *Curr. Opin. Chem. Biol.* **2002**, *6*, 742−748.
(40) Esfand, R.; Tomalia, D. A. *Drug Discovery Today* **2001**, *6*, 427−436.
(41) Medina, S. H.; El-Sayed, M. E. H. *Chem. Rev.* **2009**, *109*, 3141−3157.
(42) Mullen, D. G.; Desai, A. M.; Waddell, J. N.; Cheng, X.-m.; Kelly, C. V.; McNerny, D. Q.; Majoros, I. n. J.; Baker, J. R. Jr.; Sander, L. M.; Orr, B. G.; Banaszak Holl, M. M. *Bioconjugate Chem.* **2008**, *19*, 1748−1752.
(43) Mullen, D. G.; Fang, M.; Desai, A.; Baker, J. R. Jr.; Orr, B. G.; Banaszak Holl, M. M. *ACS Nano* **2010**, *4*, 657−670.
(44) Riva, S.; Chopineau, J.; Kieboom, A. P. G; Klibanov, A. M. *J. Am. Chem. Soc.* **2002**, *110*, 584−589.
(45) Becvar, J.; Palmer, G. *J. Biol. Chem.* **1982**, *257*, 5607−5617.
(46) Choi, J.-D.; McCormick, D. B. *Arch. Biochem. Biophys.* **1980**, *204*, 41−51.
(47) Gilli, P.; Gilli, G.; Borea, P. A.; Varani, K.; Scatturin, A.; Dalpiaz, A. *J. Med. Chem.* **2004**, *48*, 2026−2035.
(48) Patri, A. K.; Myc, A.; Beals, J.; Thomas, T. P.; Bander, N. H.; Baker, J. R. *Bioconjugate Chem.* **2004**, *15*, 1174−1181.
(49) Lafont, V.; Armstrong, A. A.; Ohtaka, H.; Kiso, Y.; Mario Amzel, L.; Freire, E. *Chem. Biol. Drug Des.* **2007**, *69*, 413−422.
(50) Zak, Z.; Ostrowski, W.; Steczko, J.; Weber, M.; Gizler, M.; Morawiecki, A. *Acta Biochim. Pol.* **1972**, *19*, 307−323.
(51) Wasylewski, M. *J. Protein Chem.* **2000**, *19*, 523−528.

(52) Wasylewski, M. *Biochim. Biophys. Acta, Proteins Proteomics* **2004**, *1702*, 137−143.